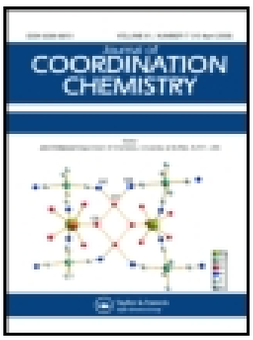

Journal of Coordination Chemistry

ISSN: 0095-8972 (Print) 1029-0389 (Online) Journal homepage: http://www.tandfonline.com/loi/gcoo20

# Spectral and computational chemistry studies for the optimization of geometry of dioxomolybdenum(VI) complexes of some unsymmetrical Schiff bases as antimicrobial agent

Mohammad Nasir Uddin, D.A. Chowdhury, Nobuyuki Mase, Mohammad Fazlur Rashid, Moniruz Zaman, Amrin Ahsan & Noor Mostaq Shah

**To cite this article:** Mohammad Nasir Uddin, D.A. Chowdhury, Nobuyuki Mase, Mohammad Fazlur Rashid, Moniruz Zaman, Amrin Ahsan & Noor Mostaq Shah (2018): Spectral and computational chemistry studies for the optimization of geometry of dioxomolybdenum(VI) complexes of some unsymmetrical Schiff bases as antimicrobial agent, Journal of Coordination Chemistry, DOI: 10.1080/00958972.2018.1533125

**To link to this article:** https://doi.org/10.1080/00958972.2018.1533125

Accepted author version posted online: 06 Oct 2018.

# Spectral and computational chemistry studies for the optimization of geometry of dioxomolybdenum(VI) complexes of some unsymmetrical Schiff bases as antimicrobial agent

MOHAMMAD NASIR UDDIN*†, D.A. CHOWDHURY†, NOBUYUKI MASE‡,
MOHAMMAD FAZLUR RASHID†, MONIRUZZAMAN†‡, AMRIN AHSAN† and NOOR MOSTAQ SHAH†

†Department of Chemistry, University of Chittagong, Chittagong-4331, Bangladesh
‡Department of Applied Chemistry and Biochemical Engineering, Shizuoka University, 3-5-1, Johoku, Hamamatsu 432-8011, Japan

This analysis highlights the design, spectroscopic characterization and quantum mechanical calculation of some new dioxomolybdenum(VI) complexes of some dibasic tetradentate Schiff bases. Ligands were derived from mono 5-bromosalicylaldehyde-orthophenylenediamine ($^{Br}$Sal-OPD) and different 2-hydroxyketone derivatives. The characterization was performed by elemental analysis, FTIR, electronic, $^{1}$H NMR and mass spectra, magnetic and molar conductance studies. Structure of the ligands and complexes were designed depending on experimental data and computational studies. According to all data, distorted octahedral geometry was proposed where oxygen atoms are in *cis* position. Prepared complexes exhibit moderate antimicrobial properties when evaluated against some pathogenic bacteria and fungi. Pharmacokinetic parameters were calculated to search their biological action, *e.g.* absorption, distribution, metabolism, excretion and toxicity.

*Keywords:* Dioxomolybdenum(VI); Dibasic tetradentate Schiff bases; Distorted octahedral geometry; Computational chemistry; pharmacokinetics



## 1. Introduction

The chemistry of transition metal complexes of Schiff bases has attracted interest in the field of bioinorganic and coordination chemistry [1]. Schiff bases containing imine group (-RC=N-) are usually formed by the condensation of primary amine or diamine with an active carbonyl compound. Every year a number of reports are published on preparation of such compounds and their applications [2-6].

*Corresponding author. Emails: nasircu72@gmail.com, mnuchem@cu.ac.bd

Schiff bases are generally bi-, tri- or tetradentate ligands capable of forming very stable complexes with transition metals [7]. Tetradentate Schiff bases with $N_2O_2$-donor atom set are well known to coordinate with various metal ions and this has attracted many reports [8]. Many symmetrical tetradentate bis-Schiff bases of 1,2-diamines with *o*-hydroxy aldehyde/ketone have been prepared and studied intensively. Keto-enol isomerism of the Schiff base *N*,*N*′-bis(salicylidene)-*o*-phenylenediamine derived by the condensation of salicylaldehyde with *o*-phenylenediamine was studied [9]. Transition metal complexes of N,N′-bis[4-(benzeneazo)salicylaldehyde]4-methyl-1,2-phenylenediamine were synthesized and characterized [10]. Nickel, copper and zinc complexes of tetradentate ligands, N,N-bis(salicylaldehyde)-*o*-phenylenediamine, N,N-bis(2-hydroxy-1-naphthaldehyde)-*o*-phenylene diamine and N,N-bis(*o*-hydroxyacetophenone)-*o*-phenylenediamine have been formed [11]. Mixed-ligand complexes of the transition metal ions Ni(II), Cu(II), Co(II), Fe(II), Mn(II), and Zn(II) with bis(4-methoxybenzylidene)-*o*-phenylinediamine (MeBen-opd) have been synthesized [12].

Less attention has been focused on unsymmetrical tetradentate Schiff bases. In particular, those derived from 1,2-diamines and different aldehydes/ketones [5, 7, 8]. Prasad *et al.* reported the synthesis of unsymmetrical Schiff base ligand from acetyl acetone with *o*-phenylenediamine as well as salicylaldehyde and their copper complexes [13]. Metal [Cu(II), Ni(II), Zn(II), Mn(II) and Co(II)] complexes of unsymmetrical tetradentate Schiff base ligand derived 5-chloro-2-hydroxybenzophenone, *o*-phenylenediamine, and salicylaldehyde have been prepared and characterized by Bi and Fan [14].

The coordination chemistry of molybdenum has assumed special importance because of its biochemical significance due to a large number of stable and accessible oxidation states [15, 16] as well as for the involvement of Mo(VI) compounds as catalysts in several industrial processes such as amoxidation of propene, epoxidation of olefins, olefin metathesis and isomerization of alicyclic alcohols [17].

This manuscript focused on Mo(IV) complexes with some unsymmetrical Schiff bases prepared from *o*-phenylinediamine and different aldehydes/ketones. Ligands and complexes are characterized with conventional methods, elemental analysis, FTIR, electronic, $^1$H NMR and mass spectra, magnetic and conductance studies. Antimicrobial properties of prepared ligands

and complexes have been investigated. Molecular modeling of the ligands and complexes has been performed by using different quantum mechanical (QM) calculations.

## 2. Experimental

### 2.1. *Materials and methods*

The diamines and sodium molybdate dehydrate were obtained from M/S E. Merck and BDH Chemicals, respectively, where others were collected from Aldrich Chemical Co. Ltd. Melting points of ligands and complexes were obtained with an electrothermal melting point apparatus. Infrared spectra on KBr pellets were recorded on a Shimadzu Infrared Spectrophotometer (model-470). Electronic spectra were run on a Shimadzu UV-Visible Spectrometer (model-1800) using 1 cm cell. $^{1}$H NMR of Schiff base ligands and their Mo(VI) complexes were recorded by a BRUKER NMR Spectrometer from Wazed Miah Science Research Center (WMSRC), Jahangirnagar University, Savar, Dhaka, Bangladesh, by dissolving samples in $CDCl_3$ or DMSO, respectively, and accordingly. Mass spectrum of several Schiff base ligands and their complexes of Mo(VI) were recorded by the process "MS Scan' through Agilent 6460 Triple Quad LC/MS' by dissolving samples in DMSO and accordingly from UL Bangladesh Ltd., Dhaka, Bangladesh. Conductivity was measured in DMF ($10^{-3}$ M) solution with a Philips Conductivity Meter (model-9501). Magnetic moment was determined at room temperature by the Gouy method.

### 2.2. *Preparation of ligands*

The tetradentate Schiff bases have been prepared by the usual condensation techniques by the following two steps.

**2.2.1. Synthesis of $^{Br}$Sal-OPD.** *o*-Phenylenediamine (OPD) and 5-bromosalicylaldehyde ($^{Br}$Sal) were added in ratio 3:1 for the preparation of mono-Schiff base ligand, $^{Br}$Sal-OPD (figure 1). OPD (40 mmol) was dissolved in 25 mL of rectified spirit (RS) to which $^{Br}$Sal (10 mmol) was added dropwise with continuous stirring in a round bottom flask fitted with a reflux condenser. The mixture was heated at 60-65 °C to reflux for 2 h and then cooled at room temperature. The product was filtered off, washed with RS, then dried and preserved in a desiccator over silica gel along with calcium chloride.

**2.2.2. Synthesis of unsymmetrical tetradentate Schiff bases.** Ethanolic solution (30 $cm^3$) of mono-(5-bromosalicyledhyde)-orthophenylenediamine ($^{Br}$Sal-OPD, 10 mmol) was added slowly with stirring to aldehyde derivatives in ethanol (30 $cm^3$). Aldehyde derivatives are 2-hydroxynapthaldehyde (HNP$\underline{H}_2$), salicylaldehyde (Sal$\underline{H}_2$), 5-chlorosalicyldehyde ($^{Cl}$Sal$\underline{H}_2$), 2-hydroxyacetophenone (HAP$\underline{H}_2$), 2-hydroxypropiophenone (HPP$\underline{H}_2$) and 2-hydroxybenzophenone (BzP$\underline{H}_2$ (figure 2). This mixture was further stirred for about 25-30 min at 50-70 °C and then cooled in an ice-bath. After about 10-12 h precipitate was separated out. This product was filtered off, washed with a small amount of ice-cooled ethanol and dried over silica gel under vacuum at room temperature.

**2.3.** ***Preparation of complexes***

**2.3.1. Preparation of bis(acetylacetonato)dioxomolybdenum, [$MoO_2(acac)_2$].** The starting material [$MoO_2(acac)_2$] was prepared by following a published procedure [18]. The compound was characterized by its metal analysis and characteristic IR and electronic spectral data.

**2.3.2. Preparation of Schiff base complexes.** The Schiff base complexes (figure 2) were prepared by reactions of [$MoO_2(acac)_2$] and the diamine Schiff base in ethanol medium by the following procedure. 5 mmol of ligand was taken in a round bottom flask containing 40 $cm^3$ of ethanol and 4 mmol of [$MoO_2(acac)_2$] was added and stirred. The mixture was refluxed for 45 min and the product was precipitated out slowly. After cooling, this was filtered off, washed with ethanol and dried under vacuum $CaCl_2$. Physical properties of prepared ligands and complexes are given in table S1 (Supplementary Material).

**2.4.** ***Estimation of Mo(VI) content***

The molybdenum content of the prepared complexes was determined by complexometric titration method after destruction of organic part of the complexes by the treatment with conc. $H_2SO_4$, conc. $HNO_3$ and 70% $HClO_4$. In acidic medium, molybdenum(VI) forms a stable complex on boiling with excess of 1,2-diaminocyclohexanetetraacetic acid (DCTA) and hydroxylamine hydrochloride. Molybdenum can then be determined by back-titration when excess DCTA was estimated with zinc chloride at pH 5-5.5 using xylenol orange as indicator. In

addition to Mo-content other elemental (C, H) analytical data of the complexes are given in table 1.

### 2.5. *Quantum mechanical (QM) methods*

The initial structure of ligands and complexes were built up and all electronic calculations were performed using Gaussian 09 program package. The QM calculation was implemented by using density functional theory (DFT) employing Becke's (B) [19] exchange functional combining Lee, Yang and Parr's (LYP) correlation functional [20] in Gaussian 09 program package for all molecules [21]. Pople's 6-31G (d) basis set was used to optimize and characterize the ligands and metal complexes which has amply been proven to give very good ground state geometries [22]. For every molecule's internal electronic energy, enthalpy, Gibb's free energy and dipole moment were calculated.

Same level of theory was used to perform the molecular orbital calculations. Hardness ($\eta$) and softness ($S$) of all drugs were also calculated from the energies of frontier HOMOs and LUMOs considering Parr and Pearson interpretation [23] of harness in DFT and Koopmans theorem [24]. Hardness ($\eta$) and softness ($S$) were calculated by using the following equations: $\eta = \frac{[\varepsilon LUMO - \varepsilon HOMO]}{2}$ ; $S = \frac{1}{\eta}$ . Partial charges of the molecules were calculated through two methods (Mulliken charge and NBO charge).

Absorption, metabolism and carcinogenic properties of all drugs were predicted by utilizing AdmetSAR online database [25]. Structure Data File (SDF) and Simplified molecular-input line-entry system (SMILES) strings were utilized throughout the generation process.

### 2.6. *Antimicrobial test*

The antibacterial tests were performed against some human pathogenic bacteria such as *Bacillus megaterium*, *Bacillus cereus*, *Bacillus subtilis*, *Salmonella typhi*, *Salmonella paratyphi*, *Escherichia coli* and four selective phytopathogenic fungi such as *Macrophomina phaseolina*, *Fusarium equisite*, *Botrydiplodiia thobrome* and *Curvularia lunata*. All strains were collected from the Department of Microbiology, University of Chittagong. The identity of all strains was confirmed.

**2.6.1. Antibacterial activities.** For the detection of antibacterial activities the disc diffusion method [26] was done. Nutrient Agar (NA) was used as the basal medium for culture of test bacteria and DMSO was used as a solvent for the initial preparation of the desired compound solution [16]. NA medium was prepared using the following composition: beef extract (3 g), peptone (5 g), NaCl (0.5 g), agar (15 g) and distilled water (1000 mL). A total of 1000 mL of distilled water was placed in a beaker and 15 g of agar powder, 3 g of beef extract, 5 g of peptone and 0.5 g of NaCl were added slowly and mixed thoroughly with a glass rod. The mixture was heated to boiling for 10 min. After 10 min of boiling, the medium was transferred to 250 mL conical flasks at a volume of 200 mL per flask. The conical flask was closed with a cotton plug and autoclaved at 121 °C and 15 psi pressure for 15 min. Culturing of different micro-organisms was then performed.

**2.6.2. Antifungal activities.** Potato Dextrose Agar (PDA) slants was prepared for maintenance and culture preservation [27]. Small portions of mycelia of the collected fungal isolates were transferred to the freshly prepared slants with the help of sterilized needles. The slants were incubated at 27±2 °C for 3 to 5 days. Glass Petri plates were sterilized and the molted sterilized PDA medium was poured at the rate 10 mL per petri plate. 0.10% solutions were prepared by dissolving 0.001 g solid samples in 1 mL DMSO. Sterilized Potato Dextrose Liquid medium (50 mL) was dispensed into 200 mL conical flasks conical flasks. Each of the flasks was labeled and 100 µL of our test compound (0.1% concentration) were added. The flasks were shaken well to mix thoroughly. Then 100 µL of 12 test samples each were added in each separate conical flask and shaken well to mix thoroughly. After that, 1 mL of fungal suspension was added carefully at each of the 13 conical flasks. All the conical flasks were incubated at 27±2 °C for 5 days. A control conical flask was prepared with DMSO solvent to observe the result.

## 3. Results and discussion

Ligands and complexes are characterized with conventional methods, elemental analysis, spectral studies (FTIR, electronic, $^{1}$H NMR and mass spectra), magnetic and conductance studies.

### 3.1. *Infrared spectra*

For the diamine Schiff bases and their complexes, the characteristic stretching modes are for ν(C=N), ν(C-O), ν(C-N) and ν(C=C). The IR spectra for the prepared ligands and complexes were taken in the range 4000-400 $cm^{-1}$. Some tentative infrared spectral band assignments characteristic to the complexes are included in table 1 and that of ligands are included in table S2. It helped to indicate regions of absorptions due to the above-mentioned vibrations. The presence of Mo-N and Mo-O vibrations confirms structural information about the coordination environment of the molybdenum. Vibration frequency of the M=O groups confirms the presence of molybdenum(VI) in the form of stable dioxocation, $[MoO_2]^{2+}$. On the basis of the FTIR studies, bands observed for the present complexes in the regions 1575-1625, 1520-1570, 1385-1460, 1350-1385 and 1250-1310 $cm^{-1}$ have been assigned as ν(C=N), aromatic ν(C=C), ν(C-C), ν(C-N) and ν(C-O), respectively. Bands near 3500 $cm^{-1}$ for ligands are characteristic of phenolic OH group. The bands appearing at 1350-1385 $cm^{-1}$ (specially the highest frequency ones near 1385 $cm^{-1}$) have been assigned to ν(C-N) [5, 6]. Again the bands appearing near 1285 $cm^{-1}$ have been assigned to ν(C-O) [2, 4]. Two sharp infrared bands for the prepared complexes in the region around 870 and 960 $cm^{-1}$ were observed due to the presence of $MoO_2$ group. Bands appearing in the regions 470-515 and 375-430 $cm^{-1}$ are assigned to Mo-N and Mo-O vibrations, respectively [3, 6, 10].

### 3.2. *Electronic spectra*

Because of the insolubility of the presently prepared complexes in common organic solvents electronic spectra of the prepared ligands and complexes were recorded in DMF. Observed bands and molar extinction coefficient (ε) values for complexes are shown in table 2. Observed bands for ligands are given in table S2. There was no evidence of any d→d transition over the visible region due to the absence of any peak above 500 nm. The observed bands lower to 300 nm of the complexes may be assignable to ligand transition. The absorption bands appearing in the energy region lower than 500 nm are attributable to a ligand to metal charge transfer (LMCT) transition.

### 3.3. *$^1$H NMR Spectra*

The $^1$H NMR spectra of the ligand $^{Br}$Sal-OPD-HAP and complexes were obtained in DMSO and $CDCl_3$ at room temperature using TMS as an internal standard. The free ligand exhibits a peak at

10.92 ppm, which is due to hydrogen-bonded phenolic protons as shown in figure 3. The chemical shift observed for the OH protons in the ligands was not observed in any of the complexes. The presence of a sharp singlet at 8.85-9.17 ppm is indicative to the -CH=N azomethine proton. The downfield shift observed in complexes is due to the de-shielding of azomethine protons as a result of the reduction of electron density after coordination. The multiplets of aromatic protons appeared within the range 7.22-8.60 ppm. The $CH_3$- and $CH_2$-proton signals are recognized at 2.50 and 3.16 ppm, respectively. $^1$H NMR assignments of the complexes are given in table 2.

### 3.4. *Mass spectrometry*

The mass specta of ($^{Br}$Sal-OPD-HAP) and [$MoO_2$($^{Br}$Sal-OPD-HAP)] show molecular ion peak at *m*/*z* = 408.4 and *m*/*z* = 534.3, respectively, which correspond to the molecular weight of the respective compounds. The series of peaks in the ranges of 108.2, 122.4, 218.3, 234.5, 322.2, 336.5 and 408.1 may correspond to various fragments of $^{Br}$Sal-OPD-HAP. Again the mass spectrum of [$MoO_2$($^{Br}$Sal-OPD-HAP)] shows peaks at 117.0, 219.1, 306.0, 360.2, 453.0, 495.1 and 534.3 may correspond to various fragments. In both cases, their intensity gives an idea of stability of these fragments. The mass spectra of [$MoO_2$($^{Br}$Sal-OPD-HAP)] is given in figure 4. The *m*/*z* values of all complexes are tabulated in table 2.

### 3.5. *Conductivity measurements*

The molar conductance values of the presently prepared complexes in DMF solution (*ca.* $10^{-3}$ M) are shown in table 2. The low conductance values (4.0-15.0 $Ohm^{-1}$ $cm^2$ $mol^{-1}$) of the prepared complexes indicate their non-electrolytic nature.

### 3.6. *Optimization of structure*

The optimized structures of ligands are labeled as L1-L6 (ligands). The molecular formula and thermochemistry of ligands like enthalpy, free energy, and electronic energy are reported in table 3. The HOMO and LUMO energies, HOMO-LUMO gap, hardness and softness of all ligands are presented in table S3. The bond distances and angles of ligands and their corresponding complexes are shown in tables S4 and S5. A comparison on experimental and theoretical IR frequencies of all ligands is shown in table S6. Selected pharmacokinetics

parameters of all ligands are reported in table S7. Optimized structures of ligands L1-L3 and their complexes are shown in figure 5. Those of other ligands and complexes are presented in figure S1. Frontier molecular orbitals, HOMO–LUMO of ligands (L1-L3) are in figure 6. Those for remaining ligands are in figure S2. Molecular electrostatic potential of all ligands and complexes are in figure 7.

**3.6.1. Thermodynamic properties.** Thermochemical data of the molecules obtained from the calculations using the same level of theories discloses the potential stability and reactivity of the molecules. Modification of ligands influences the structural properties including free energy, partial charge distribution and dipole moment [20]. More negative values are observed for the energy, enthalpy and free energies [28]. Free energy is a pivotal criterion to represent the interaction of binding partners where both the sign and magnitude are important to express the likelihood of biomolecular events occurring. Positive free energy values indicate that energy is required to drive the interaction and binding will not occur spontaneously. All the values in this inquiry are negative (table 3) meaning the binding will occur spontaneously without any extra energy expenditure. The highest free energy change is observed for L6.

**3.6.2. Frontier molecular orbital.** In the concept of frontier molecular orbitals, the term "frontier" refers to the orbitals that are at the outer edges of a molecule. These tend to be the orbitals that are the most spatially delocalized and hence, the orbitals with the highest energies (either occupied or unoccupied). In particular, two orbitals are of importance. These are the highest occupied molecular orbital or (HOMO) and the lowest unoccupied molecular orbital (LUMO). The HOMO–LUMO gap is related to the chemical hardness and softness of a molecule. "Highest" and "lowest" refer to the energies. Energy (eV) of HOMO, LUMO, HOMO-LUMO energy gap, hardness and softness of ligands and complexes are shown in table S3. Bond distances and angles of selected ligands and complexes are tabulated in tables S4 and S5, respectively. Large HOMO-LUMO gap is related to high kinetic stability and low chemical reactivity [29]. HOMO-LUMO gap, hardness and softness were calculated for the compounds and smaller the HOMO-LUMO gap increases the softness and the compound becomes more reactive. The lower frontier orbital energy gap and high dipole moment illustrates the higher reactivity of the drugs. Higher softness makes the compound more polarizable and

chemically reactive. In this analysis, it is found that L1 has lower HOMO-LUMO gap and higher softness which may contribute to its higher chemical activity than other ligands. A decreased HOMO–LUMO gap in most of the ligands promotes softness which makes them relatively more polarizable and chemically more reactive. However, for L2, there is an increase in the energy gap significantly, thus lowering the chemical reactivity. Frontier molecular orbitals, HOMO–LUMO of ligands L1-L3 have been shown in figure 6 (remaining are in figure S2).

**3.6.3. Vibrational frequency.** The vibrational band assignments were made using the Gauss-View molecular visualization program for the ligands. The spectra contain some characteristic bands of the stretching vibrations of the C-H, C-N, C-N, C-O, and C-H groups. A comparison on experimental and theoretical IR-Frequencies of all ligands is tabulated in table S6 and IR spectra obtained by the program are presented in figure S3. The aromatic structure shows the presence of C-H stretching vibrations in the region 2900-3150 $cm^{-1}$, which is the characteristic region for the identification of C-H stretching vibrations. In this region, the bands are not appreciably affected by the nature of the substituent. In the infrared spectra of the free ligands, the band observed in the region 3250-3376 $cm^{-1}$ is due to the OH group [10]. The bands observed at 1610-1625 $cm^{-1}$ are due to *v*(C=N) of the azomethine group.

**3.6.4. Molecular electrostatic potential.** For the prediction of the reactive sites for electrophilic and nucleophilic attack for the investigated compounds, molecular electrostatic potential (MEP) was calculated at B3LYP/6-31+G(d,p) optimized geometries [30]. The different values of the electrostatic potential at the surface are represented by different colors [31]; red represents regions of most electro negative electrostatic potential, blue represents regions of the most positive electrostatic potential and green represents region of zero potential. Potential decreases in the order red < orange < yellow < green < blue. The MEP surface provides necessary information about the reactive sites. The total electron density onto which the electrostatic potential surface has been mapped is shown in figure 7.

**3.6.5. Atomic partial charge.** Different methods have been proposed for assigning partial charges to the atoms of a molecule, including both quantum chemical and empirical schemes. Partial charge is an important factor for a molecule to disclose its reactivity or stability [32].

Several different methods have been proposed for assigning partial charges to the atoms of a molecule, including both quantum chemical and empirical schemes. Two different methods (Mulliken and NBO) are used here to compute the atomic partial charges of our drugs, which show positive charge when calculated with Mulliken and NBO methods [33]. Both NBO and Mulliken method have a significant role in the application of quantum chemical calculations because atomic charges affect some properties including dipole moment and polarizability. Figure S4 shows the quantum chemical calculations of atomic partial charges of all ligands and complexes.

### 3.7. *Discussion on synthesis and geometry*

Ortho-phenylenediamine (OPD) forms bis-Schiff bases with various aldehydes or ketones because of the two amino functions. But attempts of the preparation of mono-Schiff base OPD met the success. In preparing the mono-product, OPD and 5-bromosalicylaldehyde were mixed in an excess molar ratio of ortho-phenylendiamine in the ratio 1:4. The presence of excess of diamine helped the formation of mono-products instead of bis-product. In spite of our several attempts, mono-products of salicylaldehyde of o-hydoxynapthaldehyde could not be isolated due to their high solubility. This mono-product when reacted with other aldehydes or ketones gave the desired unsymmetrical bis-product. Further attempts have been made to prepare metal complexes of these unsymmetrical bis-products. It has been observed that cooling of the reaction mixture in an ice bath is necessary for easy isolation of compounds in all cases. Also heating of the solution in ethanol of the $^{Br}$Sal-OPD<u>H</u> did not change its property suggesting that mono-product did not rearrange to bis-product on heating. Rather, it helped the faster completion of the reaction. $^{Br}$Sal-OPD-HNP<u>H$_2$</u> being quite soluble in dry ethanol, product was obtained only after refluxed and then on concentration and on long cooling. $^{Br}$Sal-OPDSal<u>H$_2$</u> was obtained similarly as crystal. On the other hand $^{Br}$Sal-OPD-HAP<u>H$_2$</u> and $^{Br}$Sal-OPD-HPP<u>H$_2$</u> were obtained after reflux, concentration and long cooling in a refrigerator. Complexes are moderately soluble in most of the organic solvents but they are soluble in DMF or DMSO. The elemental analytical data confirmed [$MoO_2L$] composition that satisfied coordination requirements of Mo(VI) for an octahedral configuration. It is also supposed the tetradentate nature of the ligands coordinated through two azomethine nitrogens and two phenolic oxygens. [$MoO_2(acac)_2$] used as starting material for complexes shows an IR band at 1580 $cm^{-1}$ which is assigned to ν(C=O) due to

coordinated acetylacetone. The release of acetylacetone (acac) from $[MoO_2(acac)_2]$ after complexation forming $[MoO_2L]$ retaining the *cis*-dioxo bond was confirmed by the isolation of $[Cu(acac)_2]$ from filtrate with $Cu(CH_3COO)_2 \cdot H_2O$.

The high oxidation state +6 of molybdenum is stabilized by formation of dioxocation, $[MoO_2]^{2+}$ and the chemistry of molybdenum is dominated by this stable dioxo-species commonly referred to as molybdenum, $[MoO_2]^{2+}$ entity. The most characteristic feature of the dioxomolybdenum complexes is only one sharp and strong (O=M=O) stretching frequency observed in their infrared spectra at 900±50 $cm^{-1}$ in the case of a *trans*-$MoO_2$ group and two IR bands in the case of a *cis*-$MoO_2$ groups [34] due to the $\nu_{asym}$(O=Mo=O) and $\nu_{sym}$(O=Mo=O). The position of these two *cis*-ν(Mo=O) bands in different complexes are found to vary from ligand to ligand, indicating that the extent of location of electron cloud on Mo orbital significantly influences the Mo=O bond. The dimeric dioxomolybdenum(VI) complexes show two or more vibrational bands in this region in which there is oxygen bridged ----Mo---O---Mo--- chain interaction and the ν(Mo=O) frequency occurs at a much lower wavenumber (850 $cm^{-1}$) [35]. As two bands in the region around 870-960 $cm^{-1}$ were observed, table 3 argues the presence of a *cis*–$MoO_2$ group and the absence of any dimeric oxygen bridged chain structure which indicates the monomeric capture of these complexes. The peaks between 1580 and 1670 $cm^{-1}$ have been assigned to ν(C=N). Location of C=N band was previously described in the same region [5, 9, 10]. The band corresponding to the C=N group changed on complexation, which indicates that the azomethine nitrogen is involved in coordination [9]. The integration of aromatic OH peak is generally less than 2.0 due to intramolecular hydrogen bonding. The chemical shift observed for the OH proton in the ligands was not observed in any of the complexes. This disappearance of the singlet for the OH proton in the $^1H$ NMR spectra of the complexes indicates that the pheenolic oxygen atoms are coordinated to the central metal atom *via* deprotonation [4, 5]. Therefore, the absence of ν(O-H) bands characteristics to ligands in the complexes and negative shift of ν(C=N) indicate that the coordinated ligands acted as dinegative tetradentate ones involving coordination through two deprotonated oxygens and two azomethine nitrogens [7, 9]. The presence of a sharp singlet for the CH=N azomethine proton at 3.72 ppm of the complex showed a downfield shift in the frequency, confirming coordination of the azomethine nitrogen to central atom. This downfield shift may be assigned to the de-shielding of protons as a result of the reduction of electron density after coordination. In addition, no characteristic

acetylacetone band is present in [$MoO_2L$] complexes, indicating that no molybdenum acetylacetonate impurity is present in the prepared [$MoO_2L$] complexes.

The mass spectra of ($^{Br}$Sal-OPD-HAP) and [$MoO_2$($^{Br}$Sal-OPD-HAP)] correspond to [M+1], supporting the structure of the complexes and confirming the M:L (1:1) type stoichiometry of the metal chelates. For isotopic abundance, some fragments were found in which one or two units were less or more than the calculated value. Elemental analysis data and Mo-content also support the molecular formula as [$MoO_2L$]. The low conductance values of the prepared complexes indicate their non-electrolytic nature, indicating configuration of molybdenum in its +6 oxidation state which is satisfied by the dinegatively charged tetradentate ligand as expected.

Electronic spectral bands show no bands beyond 500 nm, indicating no d→d transition over the visible region which is expected in the molybdenum(VI) complexes having $4d^0$ configuration. The diamagnetic behavior of these complexes supports $4d^0$ electronic configuration consistent with 6+ oxidation state of the central molybdenum ion. The absorption bands lower than 500 nm are attributable to a ligand-to-metal charge-transfer [LMCT] transition. The bands in the higher energy region are attributable to $\pi\rightarrow\pi^*$ or $n\rightarrow\pi^*$ transitions within a ligand molecule. Thus, the electronic spectral data and magnetic susceptibility values clearly confirmed that the prepared complexes are genuine molybdenum(VI) species rather than molybdenum(V).

Computational chemistry study complies with the proposed structure as [$MoO_2L$]. Bond angles and distances given in tables S4 and S5 are measured from the optimized structure of the ligands and complexes. DFT has been employed to search their thermodynamic, frontier molecular orbital, vibrational frequency, atomic partial charge, equilibrium geometry and molecular electrostatic potential. All negative values are observed for the energy, enthalpy and free energies, indicating that binding will occur spontaneously without any extra energy expenditure [30]. In our analysis, it is found that L1 has lower HOMO-LUMO gap and higher softness which may contribute to its higher chemical activity than other ligands. However, there is an increase in the energy gap significantly for L2, thus lowering the chemical reactivity. The comparisons on IR frequencies of selected regions comply with experimental and theoretical values of all ligands. The characteristic region of the Schiff base derivative spectrum is 1500-1700 $cm^{-1}$ (IR spectra generated by the program are given in Supplementary Material), which is

attributed to C=N stretching vibration. The azomethine C=N stretching vibration gives rise to a band at 1638 $cm^{-1}$ in the infrared of experimental spectrum.

### 3.8. *Pharmacokinetic parameters*

Pharmacokinetic properties are calculated in AdmetSAR which predicts all compounds are non-carcinogenic [25, 36]. Pharmacokinetic parameters were calculated to search their biological action *e.g.* absorption, distribution, metabolism, excretion and toxicity. Selected pharmacokinetic parameters of all ligands and complexes are given in table S7. All ligands are P-glycoprotein non-inhibitors. P-glycoprotein inhibition can block the absorption, permeability and retention of the drugs. P-glycoprotein inhibition can block the absorption, permeability and retention of the ligands. The ligands show positive response for blood brain barrier (BBB) criteria, predicting that drugs will go through BBB. However, Schiff base ligands show non-inhibitory property for human ether-go-go-related gene (hERG). Inhibition of hERG can lead to long QT syndrome [37].

### 3.9. *Antimicrobial studies*

In the present investigation ligands and complexes have been evaluated against ten selective human pathogenic bacteria such as *Bacillus megaterium*, *Bacillus cereus*, *Bacillus subtilis*, *S. Aureus*, *Salmonella typhi*, *Salmonella paratyphi*, *S. Dysenteriae*, *P. Mutabilies*, *Escherichia coli*, *Inaba Et* and four selective phytopathogenic fungi such as *Macrophomina phaseolina*, *Fusarium equisite*, *Botrydiplodiia thobrome* and *Curvularia lunata*. The antibacterial activities of the test complexes were studied and detected by the disc diffusion method. The inhibition zones of the test organisms for different ligands and complexes are presented in table 4. It was found that almost all ligands and complexes are effective against the mentioned organisms except *Escherichia coli*. C1, C4, C5 and C6 have no inhibitory effect against it. Ligands show a bit lower inhibition than complexes. Ligands L3 and L6 show better inhibition than their respective complexes. From such observation it may be indicated that the present complex systems exhibit moderate antibacterial activity.

The percentage inhibition of mycelia growth of fungi due to the effect of studied complexes has been compared with that for a standard antibiotic, nystatine. The results are tabulated in table 5. The overall results indicate that prepared ligands and complexes showed

considerable inhibition of redial growth of mycelium against tested microorganisms. In both cases, complexes showed a bit higher inhibition than corresponding complexes. Instead results of inhibition by L3, L6 ligands and their respective complexes are comparable. Inhibition results obtained are consistent with the result of our previous experiments [4-6].

## 4. Conclusion

The unsymmetrical Schiff bases were derived by the condensation of *o*-hydroxyaldehydes (L1-L3) or ketones (L4-L6) with ortho-phenylenediamine. The prepared complexes with such ligands have been found to be [$MoO_2L$] (where $L\underline{H_2}$ = dibasic tetradentate ligands). The analytical data indicate that the complexes have 1:1 (metal:ligand) stoichiometry. Conductivity measurements indicate their non-electrolytic nature. The magnetic measurements along with electronic spectral data of the prepared complexes support $4d^0$ electronic configuration of the central metal ion consistent with the 6+ oxidation state of molybdenum ion. The infrared data indicate the presence of a *cis*-$MoO_2$ group in the complexes. The Schiff base ligands possess a planar configuration with respect to the position of the donor ONNO atoms. The [$MoO_2L$] complexes are thought to possess a distorted octahedral structure. However, exact geometry of each compound might be predicted by crystal structural evidences. AdmetSAR analysis predicts that all compounds are non-carcinogenic and ligands are P-glycoprotein non-inhibitor. It may be predicted that the prepared complexes exhibit moderate antibacterial and antifungal activity.

## References


[1] R. Ziessel. *Coord. Chem. Rev.*, **216**, 195 (2001).

[2] J. Anandakumaran, M.L. Sundararajan, T. Jeyakumar, M.N. Uddin. *Amer. Chem. Sci. J.*, **11**, 1 (2016).

[3] M.N. Uddin, D.A. Chowdhury, M.M. Rony, M.E. Halim. *Modern Chem.*, **2**, 6 (2014).

[4] M.N. Uddin, D.A. Chowdhury, K. Hossain. *J. Chin. Chem. Soc.*, **59**, 1520 (2012).

[5] M.R. Hasan, M.A. Salam, M.A. Hossain, M.N. Uddin. *J. Taibah Univ. Sci.*, **10**, 766 (2016).

[6] M.N. Uddin, S. Khandaker, Moniruzzaman, S. Amin, W. Shumi, M.A. Rahman, S.M. Rahman. *J. Mol. Struct.*, **1166**, 79 (2018).

[7] D.A. Chowdhury, M.N. Uddin, M.A.H. Sarker. *Chiang Mai J. Sci.*, **35**, 483 (2008).

[8] M.N. Uddin, M.A. Salam, M.A.B. Siddique. *Amer. J. Chem. Appl.*, **1**, 19 (2014).

[9] V.Z. Mota, G.S.G. de Carvalho, P.P. Corbi, F.R.G. Bergamini, A.L.B. Formiga, R. Diniz, M.C.R. Freitas, A.D. da Silva, A. Cuin. *Spectrochim. Acta, Part A*, **99**, 110 (2012).

[10] M. Lashanizadegan, M. Jamshidbeigi. *Synth. React. Inorg. Met-Org. Nano-Met. Chem.*, **42**, 507 (2012).

[11] M.M. Abd-Elzaher. *Synth. React. Inorg. Met-Org. Nano-Met. Chem.*, **30**, 1805 (2000).

[12] Y.J. Thakor, S.G. Patel, K.N. Patel. *J. Chem. Pharm. Res.*, **2**, 518 (2010).

[13] M.S.N.A. Prasad, G. Neeraja, B.A. Kumar, K.M. Rao, B.K. Babu, R.B. Birudu. *J. Chem. Pharm. Sci.*, **10**, 1406 (2017).

[14] C. Bi, Y. Fan. *Synth. React. Inorg. Met-Org. Chem.*, **34**, 687 (2004).

[15] S. Duman, I. Kizilcikli, A. Kaca, M. Akkurt, B. Ulkuseven. *Polyhedron*, **29**, 2924 (2010).

[16] D. Millic, V. Vrdoljak, D. Matkovic-Calogovic, M. Cinddric. *J. Chem. Crystallogr.*, **39**, 553 (2009).

[17] R.J. Cross, P.D. Newman, R.D. Peacock, D. Stirling. *J. Mol. Catal. A*, **144**, 273 (1999).

[18] T.J. Korstanje, E. Folkertsma, M. Lutz, J.T.B.H. Jastrzebski, R.J.M. Klein Gebbink. *Eur. J. Inorg. Chem.*, **12**, 2195 (2013).

[19] A.D. Becke. *Phys. Rev. A*, **38**, 3098 (1988).

[20] C. Lee, W. Yang, R.G. Parr. *Phys. Rev. B*, **37**, 785 (1988).

[21] E. Pauwels, *Uncovering Radiation Chemistry in the Solid State Through Periodic Density-Functional Calculations: Confrontation with Experimental Results and Beyond*, in: A. Lund, M. Shiotani (Eds.), Appl. EPR Radiat. Res., 667-702, Springer International Publishing (2014).

[22] H. Kruse, L. Goerigk, S. Grimme. *J. Org. Chem.*, **77**, 10824 (2012).

[23] J.L. Calais. *Int. J. Quantum Chem.*, **47**, 101 (1993).

[24] R.G. Pearson. *Proc. Natl. Acad. Sci.*, **83**, 8440 (1986).

[25] F. Cheng, W. Li, Y. Zhou, J. Shen, Z. Wu, G. Liu, P.W. Lee, Y. Tang. *J. Chem. Inf. Model.*, **52**, 3099 (2012).

[26] M.N. Uddin, D.A. Chowdhury, M.T. Islam, F. Hoque. *Orbital Elec. J. Chem.*, **4**, 273 (2012).

[27] D.A. Chowdhury, M.N. Uddin, N. Lucky. *Bull. Pure Appl. Sci.*, **22**C, 39 (2003).

[28] N.C. Garbett, J.B. Chaires. *Expert Opin. Drug Discov.*, **7**, 299 (2012).

[29] T. Stein, J. Autschbach, N. Govind, L. Kronik, R. Baer. *J. Phys. Chem. Lett.*, **3**, 3740 (2012).

[30] I. Kostova, N. Trendafilova, G. Momekov. *J. Inorg. Biochem.*, **99**, 477 (2005).

[31] D. Petrey, B. Honig. *Methods Enzymol.*, **374**, 492 (2003).

[32] A.R. Katritzky, V.S. Lobanov, M. Karelson. *QSPR: Chem. Soc. Rev.*, **24**, 279 (1995).

[33] P. Bultinck, R. Vanholme, P.L.A. Popelier, F. De Proft, P. Geerlings. *J. Phys. Chem. A*, **108**, 10359 (2004).

[34] D.A. Chowdhury, M.N. Uddin, A.K.M.L. Rahman. *Chiang Mai J. Sci.*, **33**, 357 (2006).

[35] A. Syamal. *Coord. Chem. Rev.*, **16**, 309 (1975).

[36] A. Smelcerovic, K. Tomovic, Z. Smelcerovic, Z. Petronijevic, G. Kocic, T. Tomasic, Z. Jakopin, M. Anderluh. *Eur. J. Med. Chem.*, **135**, 491 (2017).

[37] F. Montanari, M. Pinto, N. Khunweeraphong, K. Wlcek, M.I. Sohail, T. Noeske, S. Boyer, P. Chiba, B. Stieger, K. Kuchler, G.F. Ecker. *Mol. Pharm.*, **13**, 163 (2016).

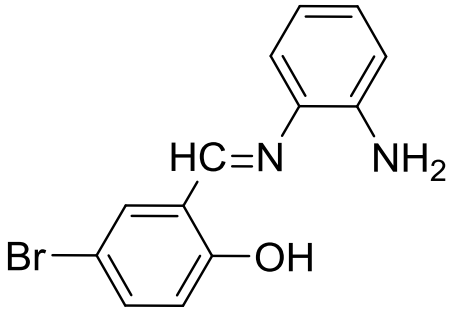


Figure 1. Structure of the ligand $^{Br}$Sal-OPD.

Ligands

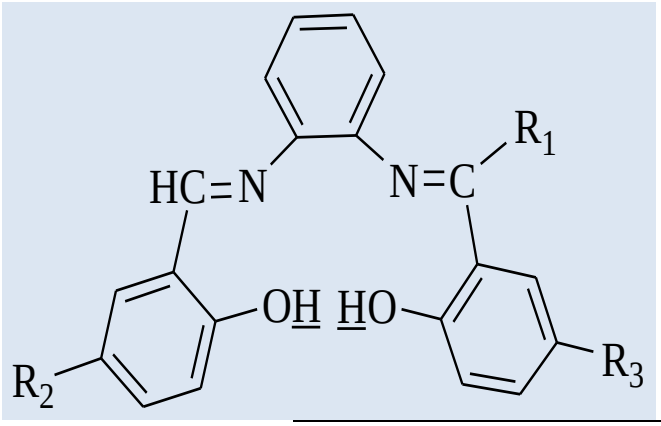


Complexes

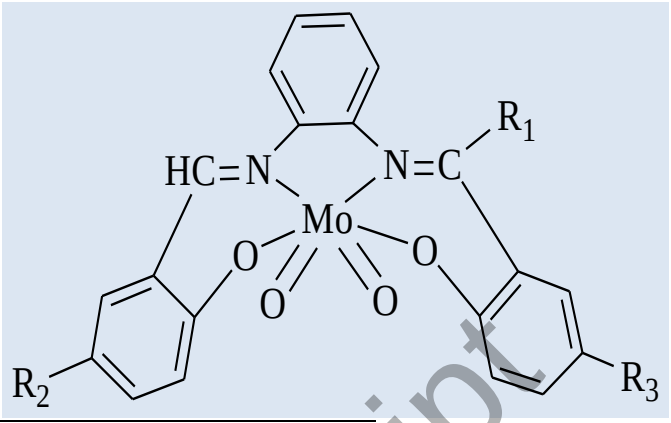


| Compound | $R_1$ | $R_2$ | $R_3$ |
|---|---|---|---|
| L1/C1 | H | Br | Fused Ph |
| L2/C2 | H | Br | H |
| L3/C3 | H | Br | Cl |
| L4/C4 | $-CH_3$ | Br | H |
| L5/C5 | $-CH_2CH_3$ | Br | H |
| L6/C6 | Ph | Br | H |

Figure 2. General structure of the ligands and their complexes.

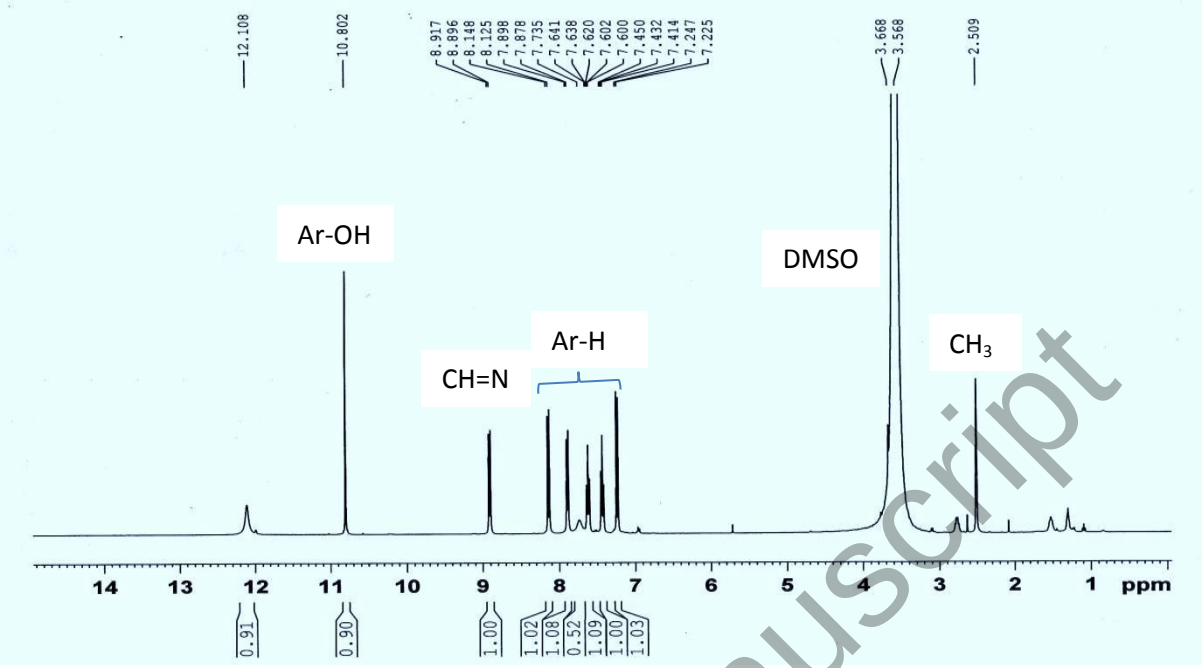


Figure 3. $^{1}$H NMR spectra of ligand $^{Br}$Sal-OPD-HAP$\underline{H}_2$.

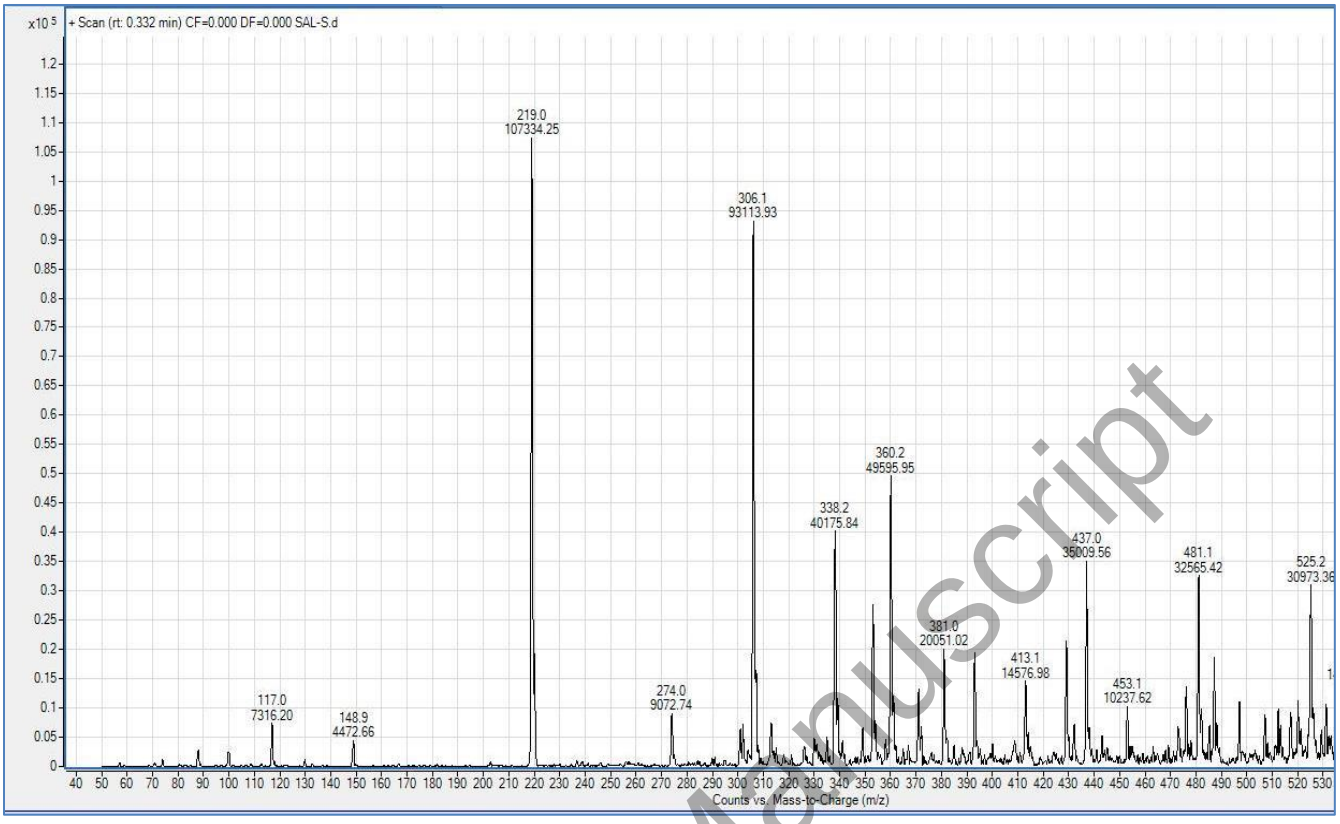


Figure 4. The mass spectra of complex [$MoO_2$($^{Br}$Sal-OPD-HAP)].

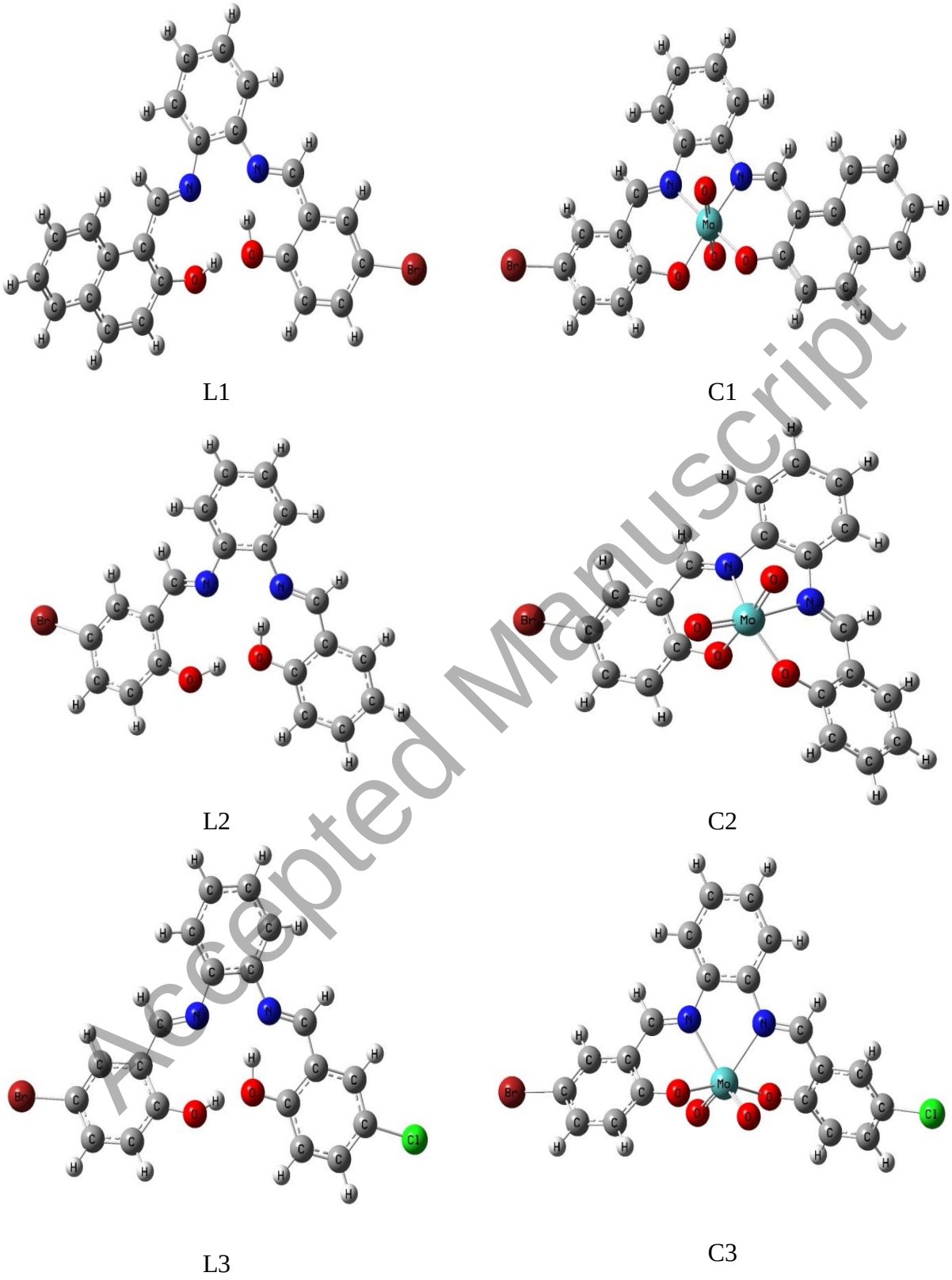




Figure 5. Optimized structure of representative ligands (L1-L3) and their complexes.

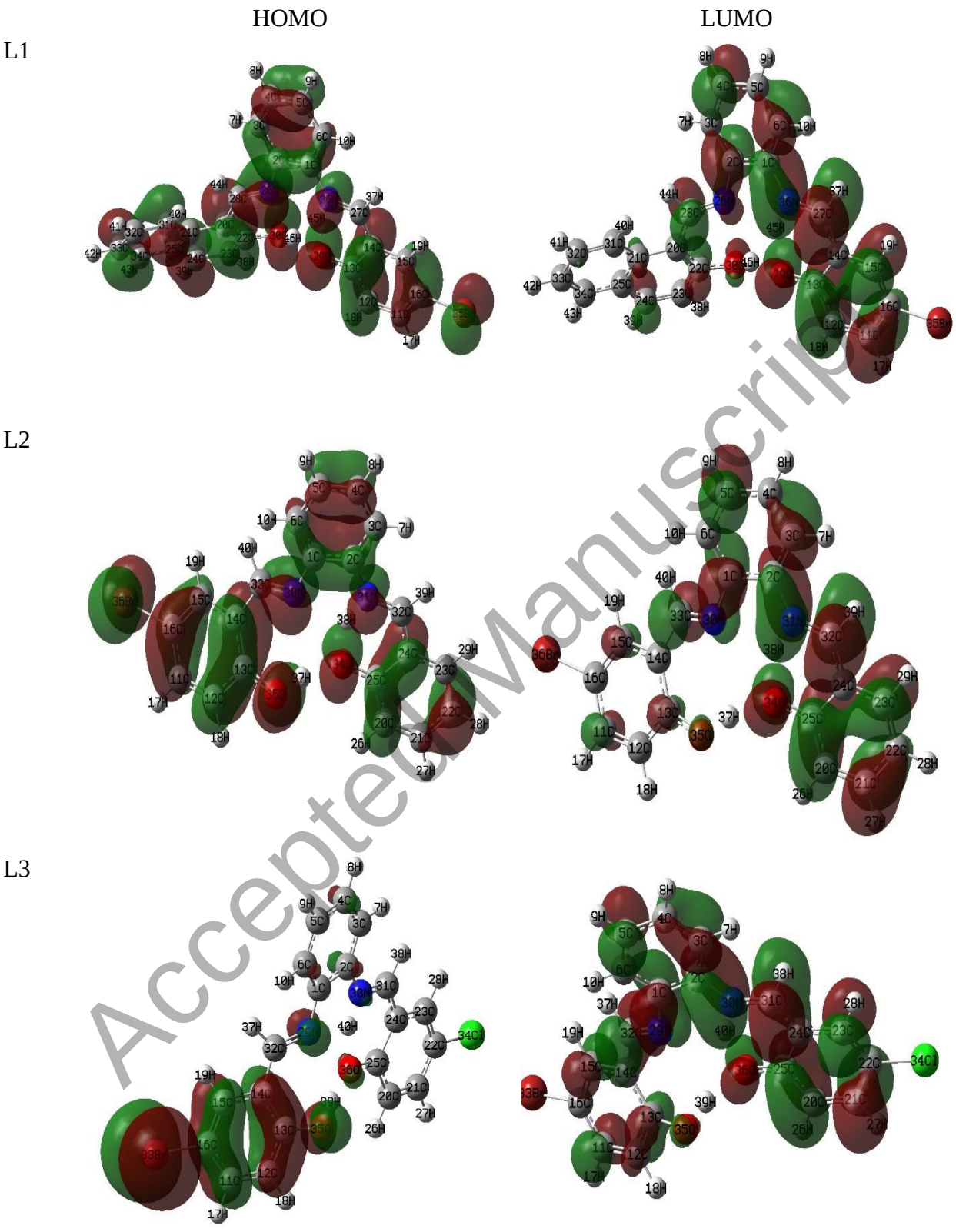




Figure 6. Frontier molecular orbitals, HOMO–LUMO of ligands (L1-L3).

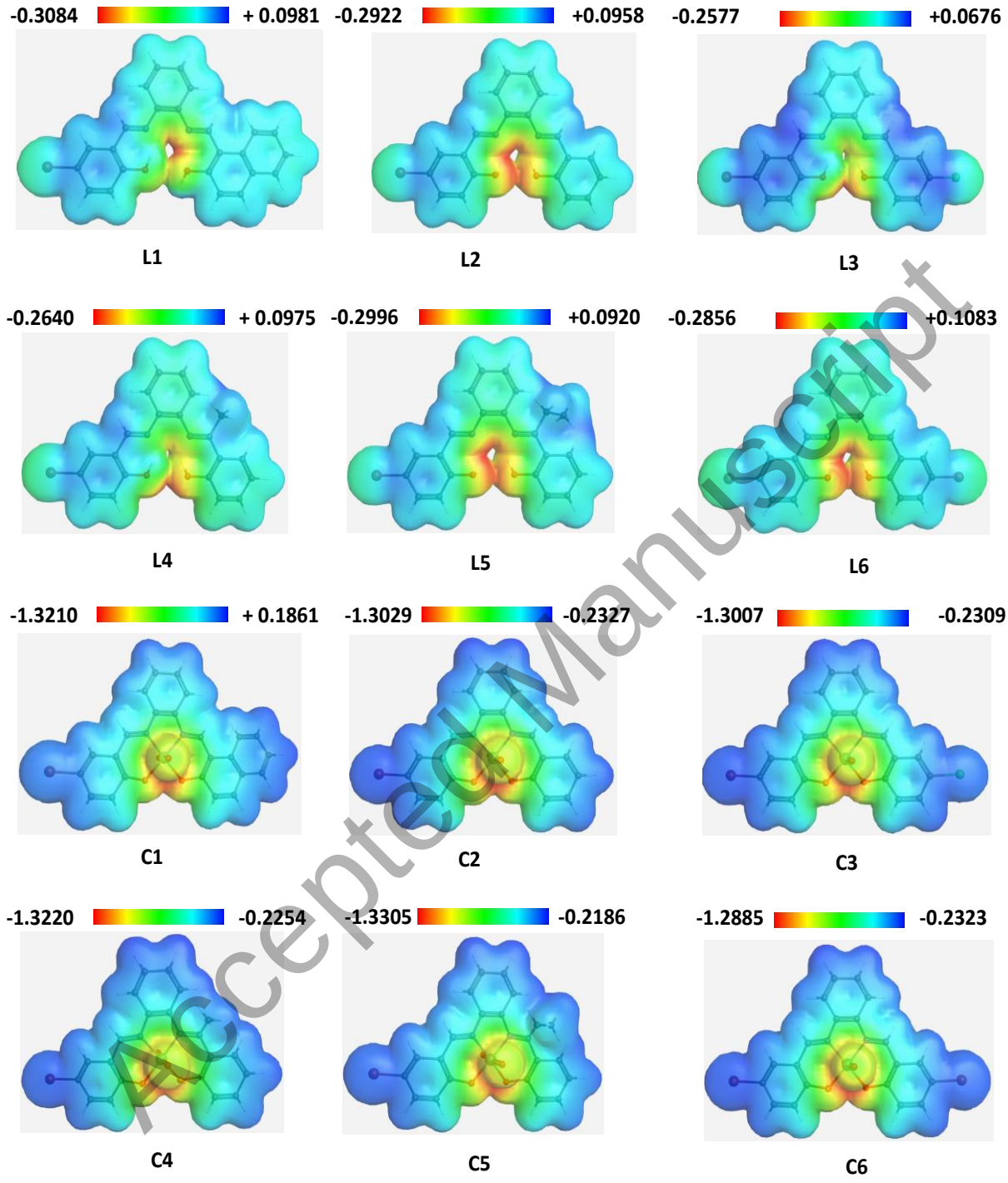


Figure 7. Molecular electrostatic potential of all ligands and complexes.

Table 1. FTIR and elemental analysis data of the complexes.

| Sl No. | Complex | Infrared spectral data ($cm^{-1}$) | | | | | | | Elemental analysis | | |
|---|---|---|---|---|---|---|---|---|---|---|---|
| | | ν(C=N) | ν(C-C) | ν(C-N) | ν(C-O) | ν(Mo=O) | ν(Mo-N) | ν(Mo-O) | % C | %H | % Mo |
| C1 | $MoO_2(^{Br}Sal$-OPD-HNP) | 1624 vs<br>1596 vs | 1425 ms | 1375 s | 1270 ms<br>1300 s | 958 vs<br>904 s | 505 w<br>475 ms | 430 ms<br>400 w | 50.52<br>(50.46) | 2.58<br>(2.65) | 14.20<br>(16.79) |
| C2 | $MoO_2(^{Br}Sal$-OPD-Sal) | 1602 vs<br>1575 s | 1430 ms<br>1420 ms | 1372<br>ms | 1285 ms | 935 vs<br>900 s | 470 s | 420 s<br>380 vs | 44.98<br>(45.87) | 2.65<br>(2.48) | 19.03<br>(18.41) |
| C3 | $MoO_2(^{Br}Sal$-OPD-$^{Cl}Sal$) | 1612 vs<br>1590 w | 1395 ms | 1350 s | 1283 vs | 945 ms<br>905 ms | 500 s<br>540 s | 400 s<br>375 s | 44.00<br>(43.23) | 2.30<br>(2.18) | 15.80<br>(17.27) |
| C4 | $MoO_2(^{Br}Sal$-OPD-HAP) | 1598 vs | 1425 ms | 1368 s | 1290 w | 950 vs<br>878 s | 515 w<br>560 ms | 410 ms | 46.73<br>(46.91) | 2.91<br>(2.80) | 20.01<br>(17.93) |
| C5 | $MoO_2(^{Br}Sal$-OPD-HPP) | 1599 vs | 1420 ms | 1370ms | 1280 s | 951 ms<br>900 s | 552 ms<br>515 s | 400 s | 48.51<br>(48.11) | 3.30<br>(3.12) | 18.90<br>(17.47) |
| C6 | $MoO_2(^{Br}Sal$-OPD-BzP) | 1612ms | 1421s | 1373 s | 1273 vs<br>1282 s | 923 vs<br>887 ms | 500 s | 415m | 52.55<br>(52.07) | 2.91<br>(2.84) | 16.20<br>(15.99) |

- Calculated values are given in parentheses
- vs = very strong, s = strong, ms = medium strong, w = weak, sh = shoulder, flsh = flat shoulder, br = broad

Table 2. $^{1}$H NMR assignments, UV-vis, conductance and mass spectral (m/z) data of the complexes.

| Complex | Chemical shift (δ) in ppm | | | Electronic spectral band (nm) | ε ($M^{-1}cm^{-1}$) | $\Lambda_m$ ($Ohm^{-1}cm^2 mol^{-1}$) | m/z |
|---|---|---|---|---|---|---|---|
| | N=CH- | Ar-H | $-CH_3$ | | | | |
| $MoO_2$($^{Br}$Sal-OPD-HNP) | 9.15 | 7.80-8.60 | --- | 390, 350, 324(sh), 270, 248, 238 | $5.5\times10^4$ | 4.0 | 573.24 |
| $MoO_2$($^{Br}$Sal-OPD-Sal) | 9.07 | 7.83-8.25 | --- | 490(flsh), 371, 313, 303, 269, 246 | $7.1\times10^4$ | 5.0 | 523.18 |
| $MoO_2$($^{Br}$Sal-OPD-$^{Cl}$Sal) | 8.85 | 7.40-8.20 | --- | 383(sh), 358, 317, 297(sh), 270 | $6.3\times10^4$ | 6.0 | 557.62 |
| $MoO_2$($^{Br}$Sal-OPD-HAP) | 9.17 | 7.88-8.45 | 2.65 | 435, 415, 385(sh), 333(sh), 320, 296 | $3.8\times10^4$ | 13.0 | 534.21 |
| $MoO_2$($^{Br}$Sal-OPD-HPP) | 9.05 | 7.62-8.46 | 2.61 | 391, 336, 313, 308, 252, 239 | $9.0\times10^4$ | 15.0 | 551.23 |
| $MoO_2$($^{Br}$Sal-OPD-BzP) | 9.21 | 7.87-8.55 | --- | 515, 373, 326(sh), 321, 272 | $5.7\times10^4$ | 9.0 | 599.28 |

- Electronic spectra and conductance data were carried out in DMF solvent.
- $^{1}$H NMR assignments were carried out in DMSO solvent.



Table 3. The molecular formula, electronic energy, enthalpy, Gibbs free energy in Hartree and dipole moment (Debye) of all ligands and complexes.

| Name | Molecular formula | Electronic energy | Enthalpy | Gibbs free energy | Dipole moment |
|---|---|---|---|---|---|
| L1 | $C_{24}H_{17}BrN_2O_2$ | -3739.687 | -3739.663 | -3739.742 | 3.880 |
| L2 | $C_{20}H_{15}BrN_2O_2$ | -3586.923 | -3586.923 | -3586.993 | 5.592 |
| L3 | $C_{20}H_{14}BrClN_2O_2$ | -4044.346 | -4044.323 | -4044.398 | 4.944 |
| L4 | $C_{21}H_{17}BrN_2O_2$ | -3626.019 | -3625.997 | -3626.072 | 6.420 |
| L5 | $C_{22}H_{20}BrN_2O_2$ | -1103.876 | -1103.855 | -1103.927 | 4.246 |
| L6 | $C_{20}H_{14}Br_2N_2O_2$ | -6148.136 | -6148.135 | -6148.212 | 4.918 |
| C1 | $C_{24}H_{15}BrN_2O_4Mo$ | -7847.140 | -7847.117 | -7847.193 | 7.729 |
| C2 | $C_{20}H_{13}BrN_2O_4Mo$ | -7694.605 | -7694.581 | -7694.658 | 7.077 |
| C3 | $C_{20}H_{12}BrClN_2O_4Mo$ | -8151.992 | -8151.967 | -8152.046 | 7.492 |
| C4 | $C_{21}H_{15}BrN_2O_4Mo$ | -7733.677 | -7733.652 | -7733.652 | 6.662 |
| C5 | $C_{22}H_{17}BrN_2O_4Mo$ | -7772.748 | -7772.721 | -7772.807 | 6.964 |
| C6 | $C_{20}H_{10}Br_2N_2O_4Mo$ | -10254.578 | -10254.555 | -10254.633 | 5.983 |

Table 4. Comparison on inhibition zones (nm) against test organisms ‘bacteria’.

| **Bacteria** | **Inhibition zone in diameter (mm)** | | | | | | | | | | | |
|---|---|---|---|---|---|---|---|---|---|---|---|---|
| | **Ligands** | | | | | | **Complexes** | | | | | |
| | L1 | L2 | **L3** | L4 | L5 | **L6** | C1 | C2 | **C3** | C4 | C5 | **C6** |
| *B. Megaterium* | 7 | 8 | **7** | 6 | 7 | **8** | 8 | 10 | **6** | 8 | 9 | **8** |
| *B. cereus* | 8 | 9 | **10** | 10 | 9 | **13** | 11 | 12 | **11** | 11 | 12 | **13** |
| *B. subtilis* | 9 | 8 | **11** | 8 | 10 | **9** | 8 | 10 | **9** | 6 | 8 | **7** |
| *S. Aureus* | 8 | 11 | **8** | 11 | 10 | **10** | 8 | 14 | **6** | 14 | 12 | **10** |
| *S. Typhi* | 8 | 10 | **10** | 6 | 6 | **7** | 10 | 12 | **10** | 7 | 8 | **7** |
| *S. Paratyphi* | 9 | 9 | **7** | 7 | 7 | **9** | 9 | 12 | **6** | 7 | 8 | **9** |
| *S. Dysenteriae* | 7 | 8 | **8** | 3 | 8 | **8** | 8 | 8 | **7** | 6 | 8 | **8** |
| *P. Mutabilies* | 15 | 13 | **24** | 16 | 13 | **22** | 20 | 16 | **25** | 18 | 16 | **22** |
| *E. Coli* | 2 | 8 | **9** | 1 | 2 | **0** | 0 | 10 | **8** | 0 | 0 | **0** |
| *Inaba Et* | 10 | 11 | **14** | 6 | 10 | **12** | 14 | 12 | **11** | 10 | 9 | **12** |

Table 5. Comparison on percentage inhibition of mycelia growth of fungi.

| Compounds | % Inhibition zone of mycelial growth of fungi | | | |
|---|---|---|---|---|
| | ***M. Phaseolina*** | ***F. Equisite*** | ***B. Theobrome*** | ***C. Lunata*** |
| L1 | 27.8 | 23.5 | 26.4 | 18.5 |
| C1 | 36.36 | 35.25 | 31.57 | 20.03 |
| L2 | 34.7 | 24.6 | 46.4 | 10.4 |
| C2 | 49.8 | 30.02 | 55.26 | 13.74 |
| L3 | 32.5 | 25.8 | 34.5 | 38.6 |
| C3 | 31.81 | 26.66 | 31.57 | 36.05 |
| L4 | 40.3 | 15.5 | 29.8 | 15.2 |
| C4 | 45.46 | 20.82 | 36.84 | 18.52 |
| L5 | 51..3 | 14.6 | 17.2 | 22.9 |
| C5 | 54.09 | 23.33 | 21.05 | 32.43 |
| L6 | 57.7 | 31.3 | 20.5 | 22.9 |
| C6 | 59.09 | 30.01 | 15.79 | 17.92 |
| Nystatine | 71.78 | 44.0 | 70.05 | 75.0 |



## Graphical abstract

**$MoO_2$($^5$BrSal-Opd-HNP)**

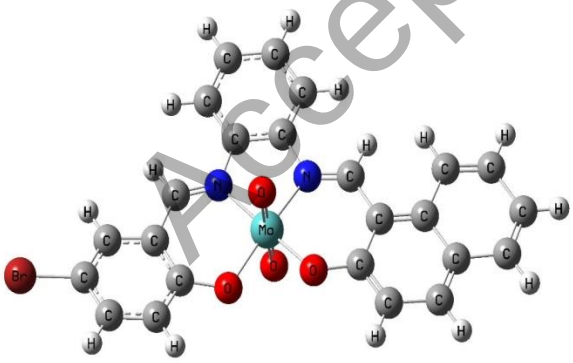

**Complexes**